Numerical Weather Prediction

Satellite Application Facility

SAF Programme

Research Report No. 2

Evaluation of the Jacobians
of infrared radiation models
for variational data assimilation

by

F. Chevallier and J.-F. Mahfouf

Abstract

In this paper, linearised versions of fast infrared radiative transfer schemes for variational data assimilation are studied. A neural network-based infrared broad-band radiation model (NeuroFlux) is compared to the European Centre for Medium-Range Weather Forecasts (ECMWF) operational radiation model. Also, a scheme for satellite brightness temperature computation (RTTOV) is compared to a more physically-based scheme: the narrow-band model Synsatrad developed at European Organization for the Exploitation of Meteorological satellites (EUMETSAT). The Jacobians are examined. They are converted into flux perturbations with the tangent-linear approximation, and into atmospheric variable increments with a one-dimensional variational assimilation system (1D-Var). For NeuroFlux as well as for RTTOV, despite accurate flux and radiance computation, the sensitivity with respect to water vapour needs to be improved.

1 Introduction

A variational algorithm adjusts a set of control variables in order to minimise a function of these variables. Variational algorithms have been increasingly used in data assimilation for numerical weather prediction. They are particularly suitable to derive statistically optimal descriptions of the atmospheric state (the so-called *analyses* of the operational weather centres) used to provide initial conditions for forecast models. In this case the function, called *cost function*, essentially consists of two terms: the first one quantifies the fit of the model state to available observations, and the second one quantifies its fit to a prior estimate (usually a short-range forecast from a previous analysis), given statistics of observation and background errors. The principle of variational data assimilation has been known for several decades (e.g., Sasaki, 1958; Lewis and Derber, 1985; Le Dimet and Talagrand, 1986). However, its high computational cost has made it operationally available only recently. At European Centre for Medium-Range Weather Forecasts (ECMWF), a three-dimensional variational assimilation system (3D-Var: Courtier *et al.*, 1998) replaced a previous scheme based on optimal interpolation (Hollingsworth, 1987) in 1996. The inclusion of the time dimension of observations in the analyses was achieved in 1997 with a four-dimensional variational assimilation system (4D-Var) as described by Courtier *et al.* (1994). An important consequence of the recent introduction of variational data assimilation in the operational weather centres is the necessity of accurate parametrisations in the analysis procedure not only in terms of atmospheric fluxes but also in terms of partial derivatives of the fluxes with respect to atmospheric variables (i.e. the Jacobians). These derivatives are needed to estimate the gradient of the cost function during the minimisation. This is placing an extra demand on modellers since it increases the requirements for the validation of physical parametrisation schemes. Moreover, a minimisation process is time-consuming when the description of the control variables is global. Therefore only fast physical parametrisations can be linearised for global variational analyses of the atmosphere. Examples of physical parametrisations for 4D-Var can be found in Janisková *et al.* (1999) and in Mahfouf (1999).

The present study examines two infrared radiation schemes for application in 4D-Var. They use different parametrisations because developments have been performed independently. The first model is a fast scheme for radiative flux computation that has been developed by Chéruy *et al.* (1996) and Chevallier *et al.* (1998). This scheme is based on artificial neural networks. The

second one is the Radiative Transfer for Tiros Operational Vertical Sounder (RTTOV: Eyre, 1991; Saunders *et al.*, 1999) for satellite radiance computation. Each scheme is validated here for variational assimilation by comprehensive comparison with a more physically-based scheme: respectively the ECMWF operational wide-band model developed by Morcrette (1991) and the narrow-band model Synsatrad (Tjemkes and Schmetz, 1997). Estimating the quality of their Jacobians is not trivial. For a better understanding of the differences, they are converted into flux perturbations with the tangent-linear approximation, and into atmospheric variable increments with a one-dimensional variational assimilation system (1D-Var), where radiation is the only physical process represented.

The plan of the paper is as follows. A description of the four infrared radiation models is given in section 2. Section 3 presents the general formalism of 4D-Var and 1D-Var. Section 4 shows the validation of the neural network-based scheme with the ECMWF operational wide-band model in a variational framework. Similarly, the comparison between RTTOV-5 and Synsatrad is detailed in section 5. Section 6 provides an overall summary.

2   Description of the radiation schemes

2.1   Two schemes for infrared broad-band flux computation

The ECMWF operational infrared broad-band radiation model (hereafter EC-OPE) computes the atmospheric fluxes and cooling rates. The cooling rates are the vertical derivatives of the net fluxes at each pressure level. As described by Morcrette (1991), the long-wave spectrum from 0 to 2820 cm^{-1} is divided in EC-OPE into six spectral regions. The integration over wavenumber is performed using a band emissivity method. The transmission functions for water vapour and carbon dioxide over the six spectral intervals of the scheme are fitted using Padé approximants on narrow-band transmissions obtained with statistical band models. Clouds are represented by multi-layer grey bodies (Washington and Williamson, 1977). Recent improvements to the scheme affect the description of the water vapour continuum and of the ice cloud optical properties, as stated by Gregory *et al.* (1998). In the ECMWF operational forecast model, radiative fluxes are currently updated once every three hours and at sample points only, in order to save time in the rather expensive radiation computations (Morcrette, 2000). However, the code is still too slow for use in the variational analysis. Therefore a very simple long-wave radiation model is used in 4D-Var. As described in Mahfouf (1999), it allows perturbations of fluxes and cooling rates to be computed with respect to temperature variations only.

In order to increase the time-space sampling, a faster version of EC-OPE, called NeuroFlux, has been derived using a statistical approach, the *multi-layer perceptron* defined by Rumelhart *et al.* (1986), together with the same cloud representation than in EC-OPE: the *multi-layer grey body model*. Consistently with the latter, upward and downward fluxes are computed in NeuroFlux as:

$$F(P_i) = \sum_k a_k F_k(P_i) \tag{1}$$

where P_i is the pressure level, F_k is the flux in the presence of a single layered black cloud in layer k or the clear sky flux (with the convention $k = 0$ for clear sky), and a_k is a weight. The a_k's are functions of the layered cloud characteristics (cloud cover, liquid and ice water

contents, particle size, ...; e.g., Ebert and Curry, 1992) and depend on the way cloudy layers overlap (e.g., Geleyn and Hollingsworth, 1979). In EC-OPE, the F_k's are computed by the method summarised at the beginning of this section, whereas artificial neural networks are used in NeuroFlux. The parameters of the neural networks are derived from EC-OPE using a non-linear regression. The set of atmospheric profiles used to define the neural network (the learning dataset) is described by Chevallier *et al.* (2000a). The validation of NeuroFlux showed that it is seven times faster than the original code while its accuracy is comparable to the accuracy of the ECMWF operational scheme, with a negligible impact on numerical simulations (Chevallier *et al.*, 2000b).

2.2   Two schemes for satellite radiance computation

The RTTOV scheme is used operationally at ECMWF for the simulation of satellite brightness temperatures. It can handle instruments like Advanced TIROS Operational Vertical Sounder (ATOVS), Special Sensor Microwave Imager (SSM/I) or Meteosat. Version 5 of this code (Saunders *et al.*, 1999) is used here. The method, originally derived from the work of McMillin *et al.* (1979), is single-band. It is based on two main approximations. The first one is that the Planck function does not vary significantly on the spectral interval considered (the spectral band of the satellite channel), so that a mean value of the Planck function can be introduced for each temperature. The second approximation is the use of a regression fitting to reference convolved line-by-line layer optical depths from the temperature and absorbing gas profiles. The reference line-by-line computations for RTTOV-5 come from GENLN2 version 4 (Edwards, 1992), with a water vapour continuum from the Clough *et al.* (1989) model, version 2.1. The temperature and absorbing gas profiles as inputs to the code are described on a fixed 43-level pressure grid.

RTTOV is compared here to Synsatrad, the narrow-band scheme developed at European Organization for the Exploitation of Meteorological satellites (EUMETSAT). This method, after Sneden *et al.* (1975), solves the monochromatic radiative transfer equation at uniformly sampled wave numbers (Tjemkes and Schmetz, 1997). The water vapour continuum refers to the Clough *et al.* (1989) model, version 2.2. The spectral resolution of the scheme depends on the channel. As an example, 750 wave numbers are used for the 6.3 μm channel on the Meteosat-7 platform, and 500 wave numbers are used for the 6.3 μm channel on High resolution Infrared Radiation Sounder (HIRS), second generation, on-board the NOAA-14 space-craft. This corresponds to resolutions of respectively 0.67 and 0.28 cm^{-1}.

The present study focuses on five channels that are of particular interest for operational weather forecasting: the water vapour sounding channels of HIRS on-board NOAA-14 at 12.5 μm (HIRS-10), 7.3 μm (HIRS-11) and 6.3 μm (HIRS-12), the water vapour sounding channel of Meteosat-7 at 6.3 μm (Meteosat-WV), and the ozone sounding channel of HIRS on-board NOAA-14 at 9.7 μm (HIRS-09). Restriction is made here to clear-sky modelling. Carbon dioxide and minor absorbing gas concentrations are set to the estimated mean level for year 2005. The surface emissivity is set to one.

3   Generalities about variational assimilation

3.1   General formalism of 4D-Var

The 4D-Var system seeks an optimal balance between observations and the dynamics of the atmosphere by finding a model trajectory $\mathbf{x}(t)$ which is as close as possible to the observations available during a given time period $[t_0, t_n]$. The model trajectory $\mathbf{x}(t)$ is completely defined by the initial state $\mathbf{x_0}$ at time t_0.

The misfit to given observations $\mathbf{y}^o$ and to an *a priori* model state $\mathbf{x}^b$ called background is measured by an objective cost-function defined as follows:

$$J(\mathbf{x_0}) = \frac{1}{2}(\mathbf{x_0} - \mathbf{x}_0^b)^T \mathbf{B}^{-1}(\mathbf{x_0} - \mathbf{x}_0^b) + \frac{1}{2}\sum_{i=0}^{n}(H_i[\mathbf{x}(t_i)] - \mathbf{y}_i)^T \mathbf{R_i}^{-1}(H_i[\mathbf{x}(t_i)] - \mathbf{y}_i) \qquad (2)$$

where at any time t_i, $\mathbf{y}_i$ is the vector of observations, H_i is the operator providing the equivalent of the data from the model variable $\mathbf{x}(t_i)$, $\mathbf{R_i}$ is the observation error covariance matrix (including measurement and representativeness errors), and $\mathbf{B}$ is the background error covariance matrix of the state $\mathbf{x}^b$. The background $\mathbf{x}^b$ is usually provided by a short-range forecast. Superscripts -1 and T denote respectively inverse and transpose matrix. The subscript i denotes the time index.

In equation (2), the observation operator H_i includes a radiative transfer model for the computation of model-equivalent satellite brightness temperatures, like RTTOV, if such quantities are assimilated.

The model state $\mathbf{x}(t_i)$ is defined as :

$$\mathbf{x}(t_i) = M(t_i, t_0)[\mathbf{x_0}] \qquad (3)$$

where M is the non-linear forecast model integrated from time t_0 to time t_i. M may include an infrared radiative transfer model for the computation of fluxes and cooling rates, like the one described in Mahfouf (1999).

The control vector $\mathbf{x_0}$ includes the prognostic variables to be initialised in the forecast model: vorticity, divergence, temperature, specific humidity and surface pressure. The minimisation uses a descent algorithm which requires several computations of the gradient of J with respect to the initial state $\mathbf{x_0}$. Given the dimension of the state vector the adjoint technique is used to provide an efficient estimate of ∇J (Le Dimet and Talagrand, 1986):

$$\nabla J(\mathbf{x_0}) = \mathbf{B}^{-1}(\mathbf{x_0} - \mathbf{x}_0^b) + \sum_{i=0}^{n} \mathbf{H_i^T R_i}^{-1}(H_i[\mathbf{x}(t_i)] - \mathbf{y}_i) \qquad (4)$$

The numerical coding of the transpose of tangent-linear versions of both the forecast model and of the observation operators H_i is required for such an efficient computation. The initial fluxes of the non-linear model around which the linearisation is performed need to be re-computed, if not stored, at each iteration of the minimisation.

3.2 General formalism of 1D-Var

The principle of the 1D-Var is similar to that of 4D-Var, but the control vector $\mathbf{x}$ represents only a single-column and the time dimension is not included. The cost-function reduces to:

$$J(\mathbf{x}) = \frac{1}{2}(\mathbf{x} - \mathbf{x}^b)^T \mathbf{B}^{-1}(\mathbf{x} - \mathbf{x}^b) + \frac{1}{2}(H(\mathbf{x}) - \mathbf{y})^T \mathbf{R}^{-1}(H(\mathbf{x}) - \mathbf{y}) \tag{5}$$

In the following, H is a radiation model, for instance RTTOV or EC-OPE. The control vector $\mathbf{x}$ contains vertical profiles of temperature, specific humidity, and ozone. Given the low dimension of the control vector, a perturbation method is used to compute the Jacobian elements of the adjoint operator $\mathbf{H^T}$ (i.e. the Jacobian matrix $\{\partial y_k / \partial x_l\}_{k,l}$). $\mathbf{H^T}$ is required to compute the gradient of the cost function:

$$\nabla J(\mathbf{x}) = \mathbf{B}^{-1}(\mathbf{x} - \mathbf{x}^b) + \mathbf{H^T}\mathbf{R}^{-1}(H(\mathbf{x}) - \mathbf{y}) \tag{6}$$

The minimiser of the present 1D-Var code is a limited memory quasi-Newton method, the M1QN3 software developed at Institut National de Recherche en Informatique et en Automatique (INRIA) (Gilbert and Lemaréchal, 1989). Examples of applications of the 1D-Var code can be found in Marécal and Mahfouf (1999) and in Fillion and Mahfouf (2000).

3.3 The background error covariance matrix

As shown in equations (2) and (5), the error covariance matrix $\mathbf{B}$ plays an essential role in 1D- and 4D-Var by determining the spatial distribution of the information on the model variables (McNally, 2000). The matrices that are used in the ECMWF 4D-Var are described by Rabier *et al.* (1998) and by Derber and Bouttier (1999). The correlations are estimated by assuming that the difference between forecasts at different ranges valid at the same time are representative of short-range forecast error statistics, as is done by Parrish and Derber (1992). Specific humidity and ozone correlations are sharp on the vertical, whereas atmospheric temperature correlations are broad in the troposphere and in the lower stratosphere with negative correlations between the two regions. No cross-correlation between the background error of temperature, specific humidity and ozone is used. Mass and wind are coupled through a linear balance operator. The standard deviations of forecast errors for temperature and ozone have been derived with the same approach, whereas the water vapour standard deviations are computed from an empirical formula (Rabier *et al.*, 1998). An example of standard deviations of temperature and humidity is given in figure 2 of Fillion and Mahfouf (2000). For temperature, they are about one degree in the troposphere with higher values in the stratosphere, up to 4.5 K. The ozone standard deviations for unbalanced quantities (i.e. the fraction of the ozone errors not coupled with wind errors) are shown in figure 1.

In the following, $\mathbf{B}$ is specified according to the operational 4D-Var for unbalanced quantities at the corresponding vertical resolutions. Two vertical resolutions are used here: the 31- and 50-level grids that have been used operationally at ECMWF respectively between 1991 and 1998, and in 1999. For ozone, standard deviations are taken from the more recent 60-level model and vertical correlations are set to zero.

4 Validation of NeuroFlux for variational assimilation

4.1 The multi-layer grey body approach in NeuroFlux

As explained in section 2.1, NeuroFlux has been derived from a non-linear regression to the ECMWF operational wide-band model (EC-OPE). In the ideal case, its computations would be identical to those of EC-OPE. In fact, the neural network parametrisation introduces some uncertainty in the fluxes and cooling rates, as well as in the Jacobians. As shown by Chevallier et al. (2000b), the accuracy of the method in terms of fluxes and cooling rates is high enough in the context of a numerical model of the atmosphere. For assimilation purposes, it is also important to have accurate Jacobians.

The Jacobians of NeuroFlux with respect to cloud characteristics are very similar to those of EC-OPE, because both schemes rely on the multi-layer grey body approach to treat cloudiness. Indeed, by differentiating equation (1), it can be written:

$$dF(P_i) = \sum_k a_k . dF_k(P_i) + F_k(P_i).da_k \tag{7}$$

The da_k's can be computed from the multi-layer grey body algorithm, with the same accuracy in NeuroFlux and in EC-OPE. This requires few computing time compared to the F_ks and dF_ks computation. As a consequence the uncertainty of the dF's computed by NeuroFlux lies in the F_k's and dF_k's. In NeuroFlux, they are computed by neural networks with comparable accuracy for each value of k.

4.2 Validation of the Jacobians

As an example of F_k, the clear-sky surface downward long-wave flux (SDLF) is considered here. The comparison between the Jacobians of the clear-sky SDLF for temperature and water vapour (i.e. the partial derivative of the flux with respect to temperature or water vapour) computed by NeuroFlux and EC-OPE is shown in figures 2a and 2b in the case of a tropical standard atmosphere (McClatchey et al., 1971). All the Jacobian elements for EC-OPE are positive which means that an increase in water vapour or temperature will increase the SDLF. Sensitivity of the SDLF to temperature is only significant near the surface and then decreases exponentially with height. Its sensitivity to specific humidity is important over a deeper layer of the lower troposphere up to 600 hPa. The decrease of the Jacobian near the surface comes from the dominance of water vapour absorption.

Compared to EC-OPE, the Jacobian of NeuroFlux for temperature appears irregular, though still close to the reference computation. The wiggles originate from the statistical approach of NeuroFlux. Indeed in a formal neural network, the information is propagated from its inputs to its outputs by non-linear projections on successive spaces, that transform and filter it. The localisation of the information, as on a pressure level grid, is partially lost. This has been already observed by Aires et al. (1999) for the modelling of HIRS brightness temperatures. The shape of the Jacobian for water vapour brings more concern. Not only the magnitude of the Jacobian below 600 hPa is underestimated, but NeuroFlux provides derivative values above 600 hPa that are higher than those of EC-OPE by several orders of magnitude. The reason of such irregularities is that, as explained by Chevallier (1998), the variables in input to the neural

networks are normalised by dividing each variable by its spread in the learning dataset. The normalised Jacobians, as illustrated on figure 2c, have limited oscillations. When projected on the physical space, using specific humidity as the water vapour variable, they convert into a chaotic profile in the upper atmosphere, where the values of specific humidity are very low.

4.3 Use of a single mean Jacobian in conjunction with NeuroFlux

The Jacobian weaknesses of NeuroFlux make it difficult to use them in variational data assimilation if significant water vapour increments are allowed by the **B** matrix (equation (2)) above 600 hPa. However, the accurate computation of finite-size perturbations of fluxes by NeuroFlux (Chevallier *et al.*, 2000b) suggests that NeuroFlux could be used to update the fluxes at each iteration of the minimisation, if a suitable Jacobian is provided by another way for the gradient computation. Such a configuration may solve the problem of computing time posed by EC-OPE.

A single mean Jacobian matrix is built as follows. The global archive of ECMWF 6-hour forecast from 1 March 1998 at 00 UTC is used to compute a mean temperature and water vapour profile, on the 31-level vertical pressure grid. The single mean Jacobian matrix is the Jacobian of this mean profile.

The association of NeuroFlux with the single mean Jacobian matrix is tested for variational assimilation. Two experiments are performed. First perturbations of cooling rates are computed. Then a 1D-Var scheme for the assimilation of surface fluxes is evaluated.

4.3.1 Impact on the computation of cooling rate perturbations

Perturbations of atmospheric temperature, specific humidity, liquid and ice water, cloud cover and surface temperature, are estimated from the difference between the 6-hour and the 12-hour ECMWF forecasts valid for the first of July 1998 at 00 UTC. The resolution is of $2.5° \times 2.5°$ (10,300 grid points). For instance, the typical size of temperature perturbations is about one degree. Perturbations of long-wave cooling rates $\delta_1\mathbf{C}$ are then computed from the model variable perturbations $\delta\mathbf{x}$: $\delta_1\mathbf{C}(\delta\mathbf{x}) = \mathbf{C}(\mathbf{x} + \delta\mathbf{x}) - \mathbf{C}(\mathbf{x})$. Figure 3 presents the mean and standard deviation of the non-linear cooling rate perturbations computed with EC-OPE, with and without cloud-radiation interaction. Three latitude classes are considered: tropical, mid-latitude and polar. Without cloud perturbations, standard deviations are below 0.5 $K.d^{-1}$, except near the surface, where they reach 1.5 $K.d^{-1}$ in average. Mean values are large only near the surface where they reach 0.3 $K.d^{-1}$ in average for tropical and mid- latitude regions. With cloud perturbations, standard deviations increase up to 3.5 $K.d^{-1}$, with some perturbations reaching up to 40 $K.d^{-1}$ (not shown).

This dataset is used to validate the single mean Jacobian approach. For the single mean Jacobian approach, as for NeuroFlux, only the accuracy of clear-sky Jacobians matters if the multi-layer grey body algorithm is used to parametrise cloud effects. Indeed, from equation (7) it appears that:

$$\delta F(P_i) \simeq \sum_k a_k.\delta F_k(P_i) + F_k(P_i).\delta a_k \qquad (8)$$

Equation (8) is a good approximation when the perturbations δF_k and δa_k are small ($|\delta F_k| << F_k$ and $|\delta a_k| << a_k$). For analysis increments, this approximation is valid for

δF_k but not for δa_k. Indeed δa_k can reach the size of a_k. But in this case $F_k(P_i).\delta a_k$ is the dominant term in equation (8), as seen by the comparison between figures 3c and 3d, which makes the approximation still accurate.

To estimate qualitatively the variations of the clear sky Jacobians, cooling rate perturbations $\delta_2 \mathbf{C}$ are computed from the temperature, specific humidity and surface temperature perturbations of the dataset, using a first-order Taylor development: $\delta_2 \mathbf{C}(\delta \mathbf{x}) = \mathbf{J}\delta \mathbf{x}$, where $\mathbf{J}$ is the single mean Jacobian matrix defined above. Figure 4 compares the clear-sky non-linear cooling rate perturbations from EC-OPE, $\delta_1 \mathbf{C}$, and the linear perturbations $\delta_2 \mathbf{C}$. The differences between the two computations originate both from the tangent-linear hypothesis and from the use of a single mean Jacobian matrix. They appear to be comparable to the signal (i.e. the non-linear perturbations shown in figure 3), except below 900 hPa in the tropical and mid- latitudes, where the standard deviation of the differences, as well as the bias, are significantly smaller than the signal. Improvement in the polar class could be obtained with a standard polar Jacobian. Because the comparison takes the tangent-linear hypothesis into account, the performance of the single mean Jacobian is underestimated. As illustrated below (section 4.3.2), the existence of a clear-sky Jacobian is important from the top of the atmosphere to the surface.

Table 1 completes this study with the statistics of the corresponding boundary fluxes: the outgoing long-wave radiation and the surface net fluxes. The error of the tangent-linear computation appears to be significantly below the signal. Indeed the error standard deviation is less than 60% of the standard deviation of the clear-sky non-linear computation in every latitude classes, with negligible biases (less than 0.2 $W.m^{-2}$).

The variability of the clear sky Jacobians does not appear to play an essential role when computing all sky flux and cooling rate perturbations. This may allow to use a single mean Jacobian with NeuroFlux for variational data assimilation. This is further investigated in the next section.

4.3.2   Impact on variational assimilation

The single mean Jacobian approach is further tested in a 1D-Var data assimilation, where only its contribution determines the increments. Use is made of observations that were collected at Billings (Oklahoma, U. S. A.) as part of the Atmospheric Radiation Measurement (ARM) program (Stokes and Schwartz, 1994). A series of five clear-sky days in December 1997 is selected to evaluate a 1D-Var assimilation of SDLF. Observations of SDLF (from a pyrgeometer) were available on a two-minute basis and were processed to get hourly averages. Corresponding hourly atmospheric profiles for temperature and specific humidity are taken from ECMWF operational short-range forecasts. The profiles as well as the background statistics (the matrix $\mathbf{B}$ of equations (2) and (5)) are described on a 31-layer vertical grid. The standard deviation of error for the SDLF is set to 10 $W.m^{-2}$ as suggested by the standard for measurements set by the Baseline Surface Radiation Network (Heimo et $al.$, 1993).

The time series of model SDLF and of SDLF from ARM observation are shown in figure 5c for the selected five days. The model systematically underestimates the observation fluxes up to 20 $W.m^{-2}$. The reader is referred to Chevallier and Morcrette (2000) for a discussion about these differences. In this context, the 1D-Var iteratively modifies the temperature and water vapour profiles in order to better match the observed SDLF within a range of background

errors given by the covariance matrix **B**.

The result of the 1D-Var assimilation using the EC-OPE radiation scheme produces a series of long-wave fluxes in better agreement with the observations as expected (figure 5c). In agreement with the vertical structure of the Jacobians (figure 2), the increase in long-wave flux has been done mostly through an increase of water vapour in the atmospheric column. The time series of the total column water vapour is shown in figure 5d.

In the single mean Jacobian approach, NeuroFlux is used in the 1D-Var to update the SDLF at each iteration of the minimisation, whereas the single mean Jacobian matrix is used to compute the gradient of the cost function. Figures 5a and 5b show that the increments of SDLF and of total column water vapour computed by the single mean Jacobian approach are in good agreement with those computed by EC-OPE. Also, the number of iterations that is needed by the 1D-Var scheme to converge is about 25% smaller with the single mean Jacobian approach than with EC-OPE. This clearly indicates that the association of NeuroFlux and of the single mean Jacobian is reasonably consistent. Moreover, the use of a pre-computed Jacobian is obviously faster than an explicit computation.

4.4   Summary

The neural network-based Jacobians contain features that are considered not to be realistic. During the learning phase of the neural networks, a non-linear regression is performed to produce accurate fluxes and cooling rates. The inclusion of the Jacobians in the non-linear regression would increase the number of constraints by two orders of magnitude. This can be achieved with more complex neural networks, but the model would then be computationally less efficient. Now, the computational burden prevents EC-OPE to be introduced in the variational analysis and faster solutions are studied. An approach is proposed for variational assimilation, in which NeuroFlux only updates the fluxes in the minimisation, or re-computes the initial ones if the incremental 4D-Var is used. The gradient computation is performed with a single mean Jacobian. Both results from 1D-Var assimilation and tangent-linear approximation show that this approach is able to provide fast computations with good accuracy.

5   Comparison between RTTOV-5 and Synsatrad

5.1   General

RTTOV and Synsatrad have been already compared for brightness temperature and Jacobian computation in the GEWEX Water Vapor Project (GVaP) where 23 models have been analysed with respect to the 6.3 μm channel on-board NOAA-14 (Soden *et al.*, 2000). It was confirmed that Synsatrad is in better agreement with line-by-line models than RTTOV. In particular, the behaviour of RTTOV Jacobians for water vapour was shown to be significantly different from that of the other models. A comparison of some 15 models in the framework of the International ATOVS Working Group (ITWG) is enlarging the comparison to six channels of HIRS. The present study completes these previous results. In addition to Eyre *et al.* (1993), who showed the positive impact of using RTTOV in the ECMWF analysis system through a 1D-Var retrieval, the present study compares its Jacobians to those from a more accurate

scheme: Synsatrad. Compared to the previous Jacobian inter-comparisons, an interpretation of the Jacobians in terms of increments of geophysical quantities, *via* the 1D-Var, is provided here.

5.2   Comparison of brightness temperatures

To compare RTTOV and Synsatrad, a representative set of atmospheric profiles is used (Chevallier, 1999). It has been obtained by a random selection of 150 situations among a large set of 13,700 carefully sampled ECMWF global 6-hour forecasts. 28 extreme profiles have been added. Unlike temperature and specific humidity, ozone comes from a climatology dependent on season and latitude (Fortuin and Langematz, 1994). In order to avoid any artefact due to orography, only profiles with a surface pressure higher than 950 hPa are used here: 103 cases. 49 of them are taken from high- and mid- latitude situations (i.e. latitudes higher than 30° in absolute value), and 54 are located in the tropical band. These profiles, defined on a 50-level vertical grid, are interpolated on the RTTOV fixed 43-level grid. Therefore, the radiation computations are performed at the same resolution for both RTTOV and Synsatrad.

Table 2 presents the comparison between RTTOV and Synsatrad for the computation of the brightness temperatures in channels HIRS-09, -10, -11, -12 and Meteosat-WV. In the high- and mid- latitude situations, mean differences are below 0.4 K with standard deviations up to 0.7 K. Differences are slightly higher for tropical latitudes, with biases and standard deviations up to 0.9 K. These numbers are comparable to the validation statistics of RTTOV-5 shown by Saunders *et al.* (1999), even if the sign of the biases may differ. Indeed, as explained in section 2.2, Synsatrad solves the monochromatic radiative transfer equation, and therefore is more accurate in principle than RTTOV-5, but is still not a line-by-line model. Differences in the reference line-by-line computations of the two schemes, like the water vapour continuum versions used (versions 2.1 and 2.2 of the Clough *et al.* -1989- parametrisation), are not likely to affect the results to a significant extent.

The higher bias occurs for Meteosat-WV in the tropics: 0.9 K. It is associated with a standard deviation of 1 K. This result is confirmed by the passive monitoring at ECMWF of the Meteosat-7 instrument, located on the equator at longitude zero. Figure 6 shows a bias of 1 K between the two schemes throughout the 40-day period presented. The bias between the radiances computed with the two schemes appears to be far more stable than the difference between the radiances observed and those derived from the model 6-hour forecast. The reader is referred to Munro *et al.* (1999) for a discussion about the differences with the observations. The Meteosat-WV bias is further investigated in section 5.4.

5.3   Comparison of 1D-Var increments

The 1D-Var scheme described in section 3.2 allows for a further comparison between RTTOV-5 and Synsatrad. The global 103 profile set is used. 1D-Var increments are computed on the 50-level grid, so that the corresponding ECMWF error statistics can be applied. A vertical interpolation scheme is provided between the minimiser and the radiation models, that are both applied on the RTTOV fixed 43-level grid.

Simulated observations are constructed by adding 1 K to the 1D-Var first-guess brightness temperature, with respect to each code. A 1 K standard deviation for the observation uncer-

tainty is specified for each channel. Tests with a 0.5 K standard deviation show similar results, differing only in the amplitude of the signals. Resulting 1D-Var increments of temperature, water vapour and ozone for each channel are examined. The conclusions for channels HIRS-11, -12 and Meteosat-WV are very similar. Therefore results for HIRS-11 and Meteosat-WV are not presented.

5.3.1   HIRS-09

As seen in table 3, the 1D-Var brightness temperature increments are small for HIRS-09, in particular in the high- and mid-latitude regions where the mean increment reaches 0.1 K only. Higher increments (0.3 K in the high- and mid-latitude regions) can be obtained if surface temperature is introduced in the 1D-Var control variables. Note that the increments would reach 1 K if no background term was specified in the cost function (equation (5)). Of course, they would be zero if the observation term was omitted. The corresponding Jacobians for ozone, shown in figure 7, peak at about 350 hPa, with higher values in the tropics than in other latitudes, whereas the maximum values of the ozone profiles, in $kg.kg^{-1}$, occur at about 10 hPa. As a consequence, HIRS-09 is mostly sensitive to a region of the atmosphere in between, about 200 hPa, where only low increments of ozone, in $kg.kg^{-1}$, are allowed in the 1D-Var because of the background term, as shown in figure 1. As shown in figure 7, the RTTOV derivative values above 400 hPa are smaller than those of Synsatrad in the tropical regions. In the other regions, they are in good agreement.

The Jacobians for temperature, not shown, have their maximum higher in altitude, about 25 hPa, with a second local maximum at about 900 hPa. The corresponding temperature increments in the 1D-Var are very small in the tropical regions, less than 0.04 K, and are higher in the other latitudes, up to 0.2 K in average, with a good agreement between RTTOV and Synsatrad (not shown).

The ozone increments are shown in figure 8. Consistently with the previous comment, the specific ozone increments peak at about 30 hPa, whereas the relative change of ozone mostly occurs at 200 hPa. As the gradient of the specified ozone error standard deviations (figure 1) is sharp at 200 hPa, the reduction of the Jacobian values above 400 hPa from Synsatrad to RTTOV makes the ozone increments smaller for RTTOV.

5.3.2   HIRS-10

The brightness temperature increments are larger for HIRS-10 than for HIRS-09: respectively about 0.30 and 0.65 K in the high and mid-latitude regions and in the tropical ones (table 3). Jacobians have their maximum in the low troposphere for the temperature and around 450 hPa for the water vapour (see figure 9 for the high and mid-latitude regions). There is no ozone absorption in this channel. Compared to Synsatrad, RTTOV-5 has smaller temperature Jacobians, and larger, somewhat irregular, water vapour ones.

The 1D-Var temperature and water vapour increments are shown in figures 10 and 11 for the high and mid-latitude regions. The shape of the temperature increments reflects the specified background error covariance matrix, that includes negative correlations between temperature errors in the lower stratosphere and those in the troposphere (section 3.3). Temperature and water vapour increments are similar for both models in value as well as in shape. The Jacobian

differences shown in figure 9 do not seem to be significant for variational data assimilation applications.

In the tropics, the brightness temperature increments are mainly due to specific humidity. Water vapour increments are similar for both schemes (not shown).

5.3.3 HIRS-12

The brightness temperature increments for HIRS-12 are similar with RTTOV and Synsatrad: between 0.75 and 0.85 K (table 3). Jacobians have their maximum at about 500 hPa for temperature and at about 250 hPa for water vapour (figure 12). If those for temperature are similar between the two models, the water vapour Jacobians have a clear distinct behaviour. RTTOV values are more than twice as high than for Synsatrad. Also, the maximum is higher in altitude with RTTOV. As expected the increment difference appears more for water vapour than for temperature (figures 13 and 14). Indeed mean relative changes of water vapour reach 40% with RTTOV at 200 hPa while not exceeding 20% with Synsatrad. Of course, these relative changes at 200 hPa correspond to small absolute amounts of water vapour (figure 14c).

5.4 Discussion

For the five channels studied (HIRS-09, -10, -11, -12 and Meteosat-WV), differences in computed brightness temperatures between the RTTOV and Synsatrad have usually less than half a degree bias and standard deviation. Jacobians for temperature appear to be in good agreement, while the width of HIRS-09 Jacobian for ozone in the tropical regions appears to be higher with Synsatrad. HIRS-11, HIRS-12 and Meteosat-WV Jacobians for water vapour are significantly different between the two codes, in shape as well as in the vertical location of the maximum. Differences reduce for HIRS-10 that peaks lower in altitude.

These differences in Jacobians translate into differences in 1D-Var increments controlled by the specified background error statistics. As a consequence, the previous increment differences are mainly specific to ECMWF, from which system these statistics were taken. In the present study, only water vapour increments for HIRS-11, HIRS-12 and Meteosat-WV significantly differ between the two models.

Due to a more physical computation method, Jacobians of Synsatrad are expected to be closer to the truth than RTTOV. Soden *et al.* (2000) also show a deficiency of HIRS-12 RTTOV Jacobians for water vapour. As described in section 2.2, RTTOV is based on two approximations: the invariance of the Planck function on the channel width and the computation of optical depths through a linear regression.

The first approximation is explored with Synsatrad as follows. Single-band convolved transmissions are computed with the narrow-band model for the five channels considered here. They are used to calculate the radiance L_i in a channel i in a way that is consistent with RTTOV-5:

$$L_i = B_i(T_{N+1})\tau_i(N+1) + \sum_{k=1}^{N} B_i(T_k)(\tau_i(k) - \tau_i(k+1)) \tag{9}$$

N is the number of vertical layers, $B_i(T)$ is the mean Planck function in channel i for temperature T, $\tau_i(k)$ is the convolved transmittance in channel i from the top of the atmosphere (level 1) to level k, T_k is mean temperature in layer k.

Statistics of the difference between the approximate brightness temperatures and the full Synsatrad computation on the 103 profile dataset are shown in table 4. Biases and standard deviations are below 0.1 K in absolute value for all channels, except for Meteosat-WV, where a bias of 0.5 K is found. This bias carries the same sign as the one between RTTOV and Synsatrad, but is not latitude-dependent as the latter (see table 2). Indeed different sources of error add or compensate between RTTOV and Synsatrad. Table 4 suggests that the invariant-Planck-function approximation is important to explain the differences observed for Meteosat-WV. This is not surprising given the Meteosat-WV spectral width, ranging from 1350 to 1850 cm^{-1}, to be compared with HIRS-12 ranging between 1420 to 1560 cm^{-1} only. The low associated standard deviation (0.1 K) suggests that a simple bias correction is able to remove that particular problem. As far as the Jacobians are concerned, only small impact is found on Meteosat-WV as well as on HIRS-12 (not shown).

Therefore the second approximation on which RTTOV relies, namely the use of a linear regression to derive the optical depths, is likely to be responsible for the low accuracy of RTTOV 6.3μm and 7.3μm water vapour Jacobians. Tests have been performed to use a non-linear regression (neural networks) for brightness temperature computation. They are illustrated on figure 15. Jacobians for water vapour are not any better than those of RTTOV, whereas Jacobians for temperature are slightly less accurate. Thus improvements of RTTOV may be expected more from a better quality of the regression dataset (e.g., Chevallier, 1999) and from more adequate predictors (e.g., Matricardi and Saunders, 1999). The interpolation of the water vapour profiles of the current regression dataset between 100 and 300 hPa (as explained by Saunders *et al.*, 1999) may be the main reason for the bad Jacobians (R. Saunders, personal communication, 2000; see also figure 12b).

6   Conclusion

Variational methods are increasingly used for data assimilation in operational weather centres. They provide statistically optimal analyses of the atmosphere when error statistics and Jacobians are correctly specified. The evaluation of Jacobians for variational data assimilation has to be related to the complete framework including the specified error statistics. As an example, the differences between RTTOV and Synsatrad Jacobians were shown to be strongly influenced by these statistics when they are converted into 1D-Var increments.

Neural network-based Jacobians for broad-band infrared radiation were shown to be deficient for water vapour. However, the random structure of the derivative error allows to use NeuroFlux with a single mean Jacobian in the variational context. Errors produced by this approach are small. Clouds are the major modulator of fluxes and cooling rates and are accounted for in the framework of the multi-layer grey body approach. Therefore, accurate and fast long-wave broad-band radiation computations can be introduced in 4D-Var with the single mean Jacobian approach to compute increments and derivatives, and NeuroFlux to re-compute the trajectory around which the linearisation is performed.

For satellite brightness temperature modelling, RTTOV Jacobians were also shown to be deficient for water vapour for the 6.3 μm and 7.3 μm channels with a significant impact on the 1D-Var retrievals. The mean shape of the increments are similar to those of Synsatrad, but the signal amplitude differs. This may explain why the inclusion of RTTOV in variational

data analysis for the assimilation of such channels positively impacts the quality of the operational analyses and forecasts, particularly in the southern hemisphere and tropics (McNally and Vespérini, 1996). Smaller weaknesses for temperature and ozone, as well as for water vapour in the 12.5 μm channel (HIRS-10) do not significantly impact the increments. Further improvements to RTTOV are expected from on-going work in the framework of the Numerical Weather Prediction Satellite Application Facility (NWP/SAF) funded by Eumetsat, where both the regression data-set and the choice of the predictors are being revised.

Acknowledgements

References

Aires, F., M. Schmitt, A. Chédin, and N. A. Scott, 1999: The "weight smoothing" regularization of MLP for Jacobian stabilization. *IEEE Trans. Neural Networks*, **10:6**, 1502:1510.

Chéruy, F., F. Chevallier, J.-J. Morcrette, N. A. Scott, A. Chédin, 1996 : Une méthode utilisant les techniques neuronales pour le calcul rapide de la distribution verticale du bilan radiatif thermique terrestre. *C. R. Acad. Sci. Paris*, **322:IIb**, 665-672, in French.

Chevallier, F., 1998: La modélisation du transfert radiatif à des fins climatiques : une nouvelle approche fondée sur les réseaux de neurones artificiels. PhD thesis, University Paris VII, 230 pp. [Available from LMD, Ecole Polytechnique, 91128 Palaiseau cedex, France].

Chevallier, F., 1999: TIGR-like sampled databases of atmospheric profiles from the ECMWF 50-level forecast model. *ECMWF/Eumetsat NWP SAF Research Report No. 1*, 18 pp.

Chevallier, F., F. Chéruy, N. A. Scott, and A. Chédin, 1998: A neural network approach for a fast and accurate computation of longwave radiative budget. *J. Appl. Meteor.*, **37**, 1385-1397.

Chevallier, F., and J.-J Morcrette, 2000: Comparison of model fluxes with surface and top-of-the-atmosphere observations. *Mon. Wea. Rev.*, in press.

Chevallier, F., A. Chédin, F. Chéruy, J.-J. Morcrette, 2000a: TIGR-like atmospheric situation databases for accurate radiative flux computation. *Quart. J. Roy. Meteor. Soc.*, **126**, 777-785.

Chevallier, F., J.-J Morcrette, F. Chéruy, and N. A. Scott, 2000b: Use of a neural network-based longwave radiative transfer scheme in the ECMWF atmospheric model. *Quart. J. Roy. Meteor. Soc.*, **126**, 761-776.

Clough, S. A., F. X. Kneizys, and R. Davies, 1989: Line shape and the water vapor continuum. *Atmos. Res.*, **23**, 229-241.

Courtier, P., J.-N. Thépaut, and A. Hollingsworth, 1994: A strategy, for operational implementation of 4D-Var, using an incremental approach. *Q. J. Roy. Meteor. Soc.*, **120**, 1367-1388.

Courtier, P., E. Andersson, W. Heckley, J. Pailleux, D. Vasiljević, M. Hamrud, A. Hollingsworth, F. Rabier, and M. Fisher, 1998: The ECMWF implementation of three dimensional variational assimilation (3D-Var). Part I.: formulation. *Q. J. Roy. Meteor. Soc.*, **124**, 1783-1808.

Derber, J. and F. Bouttier, 1999: A reformulation of the background error covariance in the ECMWF global data assimilation system. *Tellus*, **40A**, 1-25.

Ebert, E. E. and J. A. Curry, 1992 : A parameterization of ice optical properties for climate models. *J. Geophys. Res.*, **97D**, 3831-3836.

Edwards, D. P., 1992: GENLN2. A general line-by-line atmospheric transmittance and radiance model. Technical note NCAR/TN-367+STR, National Center for Atmospheric Research, Boulder, Co.

Eyre, J. R., 1991: A fast radiative transfer model for satellite sounding systems. *ECMWF Technical Memorandum No. 186*.

Eyre, J. R., G. A. Kelly, A. P. McNally, E. Andersson, and A. Persson, 1993: Assimilation of TOVS radiance information through one-dimensional variational analysis. *Q. J. Roy. Meteor. Soc.*, **119**, 1427-1463.

Fillion, L., and J.-F. Mahfouf, 2000: Coupling of moist-convective and stratiform precipitation processes for variational data assimilation. *Mon. Wea. Rev.*, **128**, 109-124.

Fortuin, J. P. F. and Langematz, U., 1994: An update on the global ozone climatology and on concurrent ozone and temperature trends. *Proceedings SPIE*, 2311, 207-216.

Geleyn, J.-F. and A. Hollingsworth, 1979 : An economical analytical method for the computation of the interaction between scattering and line absorption in radiation. *Beitr. Phys. Atmosph.*, 52, 1-16.

Gilbert, J. C., and C. Lemaréchal, 1989: Some numerical experiments with variable-storage quasi-Newton algorithms. *Mathematical Programming*, **45**, 407-435.

Gregory, D., J.-J. Morcrette, C. Jakob, and A. Beljaars, 1998: Introduction of revised radiation, convection, cloud and vertical diffusion schemes into Cy18r3 of the ECMWF integrated forecasting system. ECMWF Technical Memorandum No. 254.

Heimo, A., A. Vernez, and P. Wasserfallen, 1993: Baseline Surface Radiation Network (BSRN). Concept and implementation of a BSRN station. WMO/TD No. 579, WCRP/WMO, Geneva.

Hollingsworth, A, 1987: Objective analysis for numerical weather prediction. *Short and medium range numerical weather prediction, Special Volume J. Met. Soc. Jap.*, Matsumo, T., Ed., 11-60.

Janisková, M., J.-N. Thépaut and J.-F. Geleyn, 1999: Simplified and regular physical parameterizations for incremental four-dimensional variational assimilation. *Mon. Wea. Rev.*, **127**, 26-45.

Le Dimet, F.-X. and O. Talagrand, 1986 : Variational algorithms for analysis and assimilation of meteorological observations. *Tellus*, **38A**, 97-110

Lewis, J. M. and J. C. Derber, 1985: The use of adjoint equations to solve a variational adjustment problem with advective constraints. *Tellus*, **37A**, 309-322.

Mahfouf, 1999: Influence of physical processes on the tangent-linear approximation. *Tellus*, **51A**, 147-166.

Marécal, V., and J.-F. Mahfouf, 1999: Variational retrieval of temperature and humidity profiles from TRMM precipitation data. *ECMWF Technical Memorandum No. 293*.

Matricardi, M., and R. Saunders, 1999: Fast radiative transfer model for simulation of infrared atmospheric sounding interferometer radiances. *Appl. Opt.*, **38:27**, 5679:5691.

McClatchey, R. A., R. W. Fenn, J. E. A. Selby, F. E. Volz, and J. S., Garing, 1971: Optical properties of the atmosphere. Technical Note No. AFCRL-TR-73-0096, Air Force Cambridge Res. Lab., Bedford, Mass.

McMillin, L. M., H. E. Fleming, M. L. Hill, 1979: Atmopsheric transmittance of an absorbing gas. 3: a computationally fast and accurate transmittance model for absorbing gases with variable mixing ratios. *Appl. Opt.*, **18**, 1600-1606.

McNally, A. P., 2000: Estimates of short-range forecast-temperature error correltions and the implications for radiance-data assimilation. *Q. J. Roy. Meteor. Soc.*, **126**, 361-373.

McNally, A. P., and M. Vespérini, 1996: Variational analysis of humidity information from TOVS radiances. *Q. J. Roy. Meteor. Soc.*, **122**, 1521-1544.

Morcrette, J.-J., 1991: Radiation and Cloud Radiative Properties in the European Center for Medium Range Weather Forecasts forecasting system. *J. Geophys. Res.*, **96:D5**, 9121-9132.

Morcrette, J.-J., 2000: On the effects of the temporal and spatial sampling of radiation fields on the ECMWF forecasts and analyses. *Mon. Wea. Rev.*, **128**, 876-887.

Munro, R., G. Kelly, and R. Saunders, 1999: Assimilation of Meteosat Radiance Data within the 4DVAR System at ECMWF. EUMETSAT/ECMWF Fellowship Programme Report.

Parrish, D. F. and J. C. Derber, 1992: The National Meteorological Center's Spectral Statistical Interpolation Analysis System. *Mon. Wea. Rev.*, **120**, 1747-1763.

Rabier, F., A. McNally, E. Andersson, P. Courtier, P. Unden, J. Eyre, A. Hollingsworth and F. Bouttier, 1997 : The ECMWF implementation of three dimensional variational assimilation (3D-Var). Part II : Structure functions. *Q. J. Roy. Meteor. Soc.*, **124**, 1809-1829.

Rabier, F., H. Järvinen, E. Klinker, J.-F. Mahfouf and A. Simmons, 2000: The ECMWF operational implementation of four dimensional variational assimilation. Part I : Experimental results with simplified physics. *Q. J. Roy. Meteor. Soc.*, 1143-1170.

Rumelhart, D. E., G. E. Hinton, and R. J., Williams, 1986: Learning internal representations by error propagation. *Parallel distributed processing: Explorations in the macrostructure of cogn ition 1*, D. E. Rumelhart and McClelland, Eds., MIT Press, 318-362.

Sasaki, Y., 1958: An objective analysis based on the variational method. *J. Meteor. Soc. Japan*, **36**, 738-742.

Saunders, R., M. Matricardi, and P. Brunel, 1999: An improved fast radiative transfer model for assimilation of satellite radiance observations. *Quart. J. Roy. Meteor. Soc.*, **125:556**, 1407-1425.

Sneden, C., H. Johnson, and B. Krupp, 1975: A statistical method for treating molecular line opacities. *Astrophys. J.*, **204**, 281-289.

Soden, B. and co-authors, 2000: An intercomparison of radiation codes for retrieving upper tropospheric humidity in the 6.3 micron band: a report from the 1st GVaP workshop. *Bull. Amer. Meteo. Soc.*, **81**, 797-808.

Stockes, G. M., and S. E. Schwartz, 1994: The Atmospheric Radiation Measurement (ARM) Program: programmatic background and design of the cloud and radiation testbed. *Bull. Amer. Meteo. Soc.*, **75**, 1201-1221.

Tjemkes, S. A. and J. Schmetz, 1997: Synthetic satellite radiances using the radiance sampling method. *J. Geophys. Res.*, **102D**, 1807-1818.

Washington, W. M. and D. L. Williamson, 1977 : A description of the NCAR GCM's in General circulation models of the atmosphere. *Methods in Computational Physics*, J. Chang. Ed., 17, Academic Press, 111-172.

(a) Outgoing long-wave radiation

	polar		mid-latitude		tropical	
	M	σ	M	σ	M	σ
TL - NL clear sky	-0.02	0.70	0.03	1.20	-0.14	1.46
NL clear sky	-0.13	1.49	-0.19	2.36	0.11	2.84
NL total sky	0.11	5.71	-0.19	11.78	0.74	17.27

(b) Surface net long-wave flux

	polar		mid-latitude		tropical	
	M	σ	M	σ	M	σ
TL - NL clear sky	-0.04	1.75	0.01	0.64	0.15	1.00
NL clear sky	0.16	2.94	0.04	4.52	-0.19	3.86
NL total sky	1.36	10.57	0.39	13.69	0.39	9.57

Table 1: First row of each table shows the mean (M) and standard deviation (σ) of the comparisons between tangent-linear (TL) and non-linear (NL) clear sky outgoing long-wave radiation and clear sky surface net flux perturbations. Middle row shows the mean and standard deviation of the NL clear sky flux perturbations. Bottom row shows the mean and standard deviation of the NL total sky flux perturbations. The perturbations are taken from the difference between the ECMWF 6- and 12- hour forecasts for 1 July 1998 at 00 UTC. The fluxes are in $W.m^{-2}$. Results are shown in three latitude classes.

(a) High and mid-latitudes

	HIRS-09		HIRS-10		HIRS-11		HIRS-12		MET. WV	
	M	σ	M	σ	M	σ	M	σ	M	σ
RTTOV-5 - Synsatrad	-0.3	0.4	-0.1	0.2	0.4	0.4	0.3	0.7	0.0	0.7
Synsatrad	249.9	13.3	267.5	14.6	251.3	7.4	239.3	6.3	239.1	6.3

(b) Tropical latitudes

	HIRS-09		HIRS-10		HIRS-11		HIRS-12		MET. WV	
	M	σ	M	σ	M	σ	M	σ	M	σ
RTTOV-5 - Synsatrad	-0.6	0.1	-0.5	0.3	-0.1	0.5	-0.2	0.9	-0.9	1.0
Synsatrad	274.3	3.0	287.4	3.1	261.2	4.5	245.5	6.1	245.5	6.0

Table 2: Statistics of the comparison of Synsatrad and RTTOV-5 for the computation of brightness temperatures, in K.

(a) High and mid-latitudes

	HIRS-09	HIRS-10	HIRS-11	HIRS-12	MET. WV
Mean δT_b RTTOV-5	0.10	0.29	0.64	0.80	0.81
Mean δT_b Synsatrad	0.11	0.30	0.62	0.75	0.75

(b) Tropical latitudes

	HIRS-09	HIRS-10	HIRS-11	HIRS-12	MET. WV
Mean δT_b RTTOV-5	0.28	0.66	0.78	0.84	0.84
Mean δT_b Synsatrad	0.31	0.63	0.77	0.83	0.83

Table 3: Mean brightness temperature increment (δT_b) of the 1D-Var using either RTTOV-5 or Synsatrad.

	High and mid-lat.		Tropical latitudes	
	M	σ	M	σ
HIRS-09	-0.1	0.0	-0.1	0.0
HIRS-10	0.0	0.0	0.0	0.0
HIRS-11	0.1	0.0	0.1	0.0
HIRS-12	-0.2	0.1	-0.1	0.1
Meteosat WV	-0.5	0.1	-0.5	0.1

Table 4: Test of the impact of the spectral integration approximation used in RTTOV. Difference between the computation of brightness temperature with Synsatrad in the narrow-band mode and that with Synsatrad using the approximation (approximation minus narrow-band, in K).
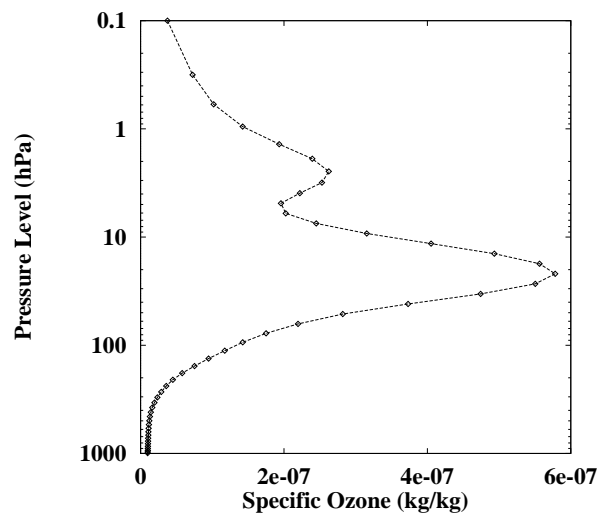
Figure 1: Profile of background error standard deviations for unbalanced ozone.
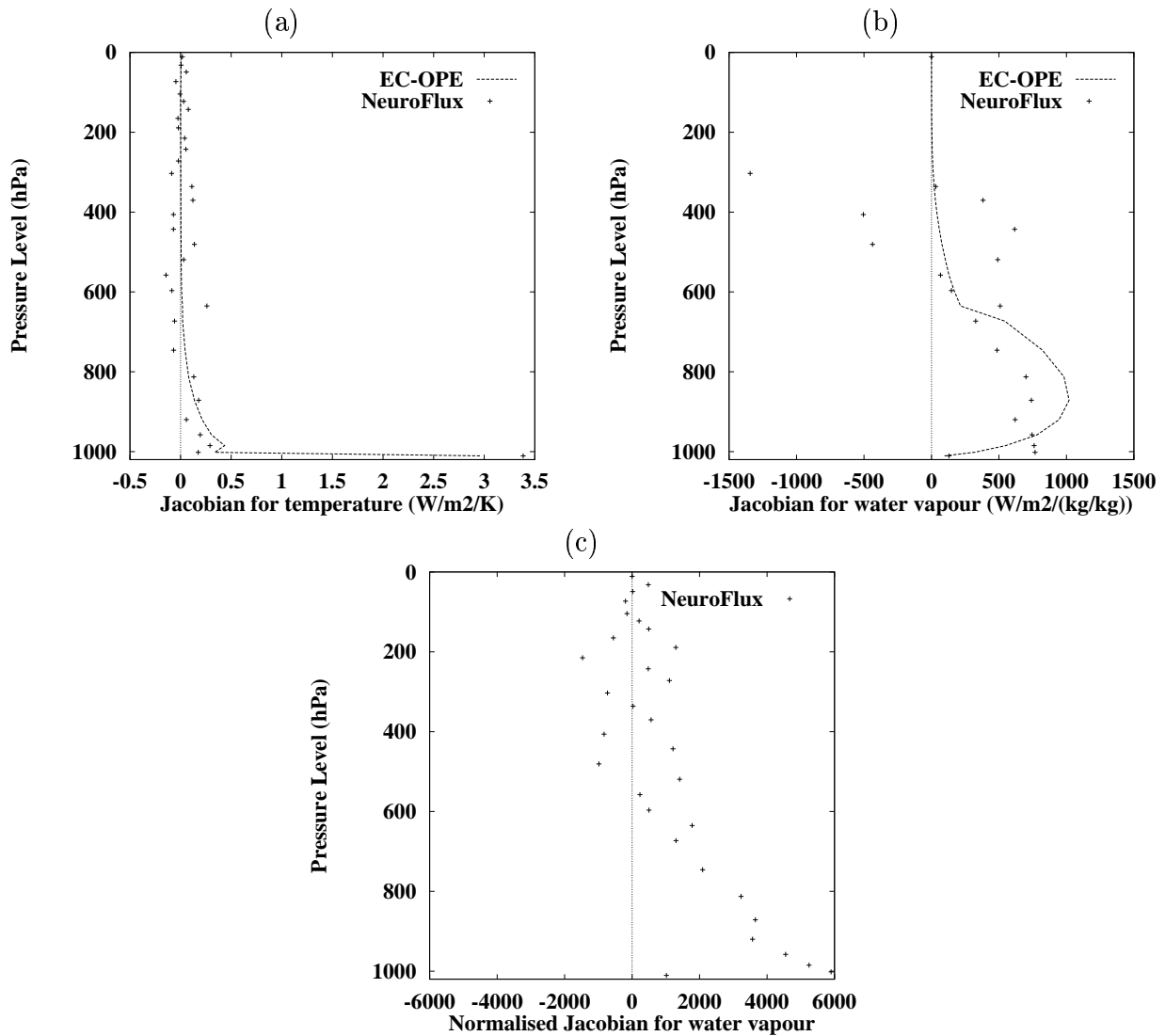
Figure 2: Jacobians of surface downward flux for temperature (a) and water vapour (b) as calculated by EC-OPE and NeuroFlux for the standard tropical atmosphere. The higher part of the neural network Jacobian for water vapour does not appear because NeuroFlux provides values above 300 hPa that are higher than those of EC-OPE by several orders of magnitude. The neural network Jacobian for water vapour, normalised in the neural network space, is shown in (c).

(a) Mean

(b) Mean

(c) Standard deviation

(d) Standard deviation
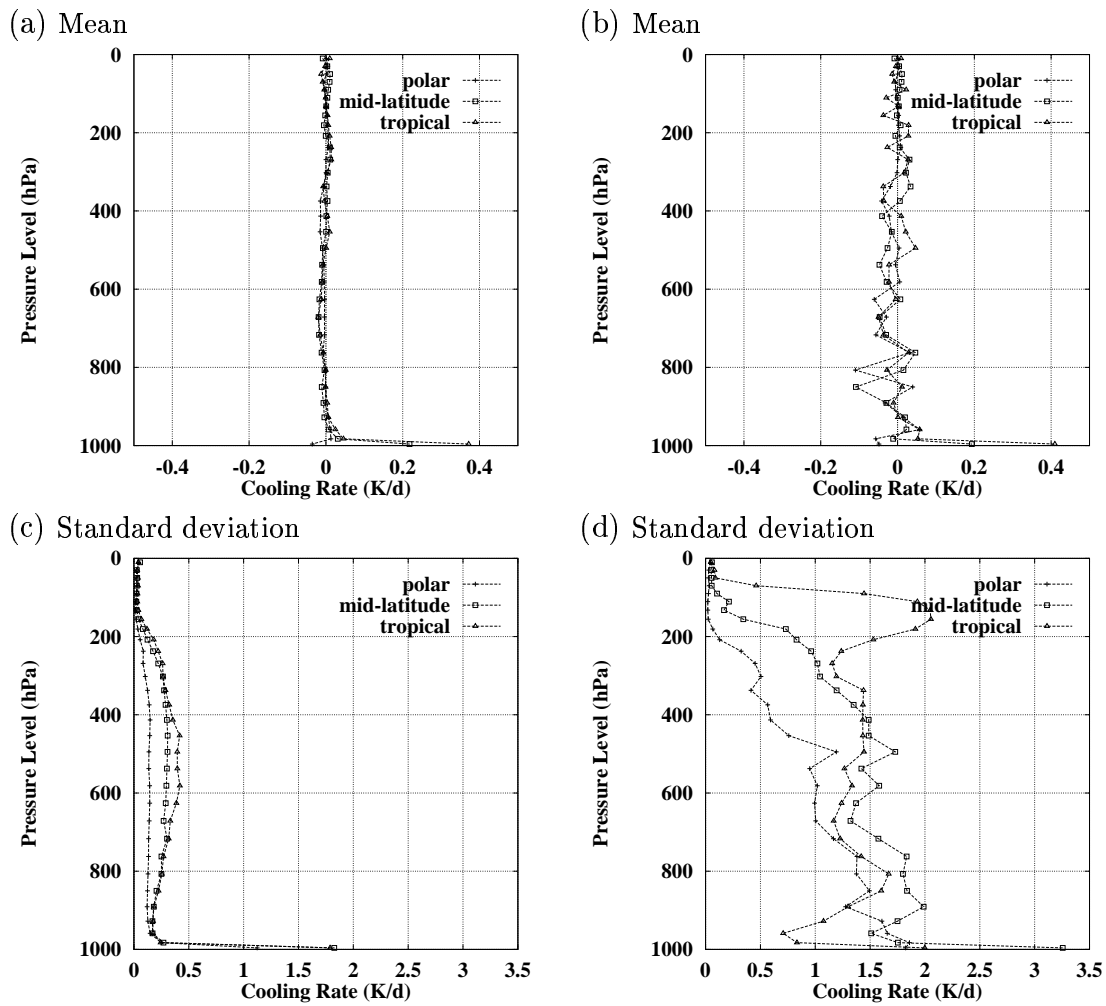
Figure 3: Mean (top row) and standard deviation (bottom row) of the clear sky (left column) and the total sky (right column) non-linear cooling rate perturbations, in $K.d^{-1}$. The perturbations are taken from the difference between the ECMWF 6- and 12- hour forecasts for 1 July 1998 at 00 UTC. Results are shown in three latitude classes.

(a) Bias

(b) Standard deviation
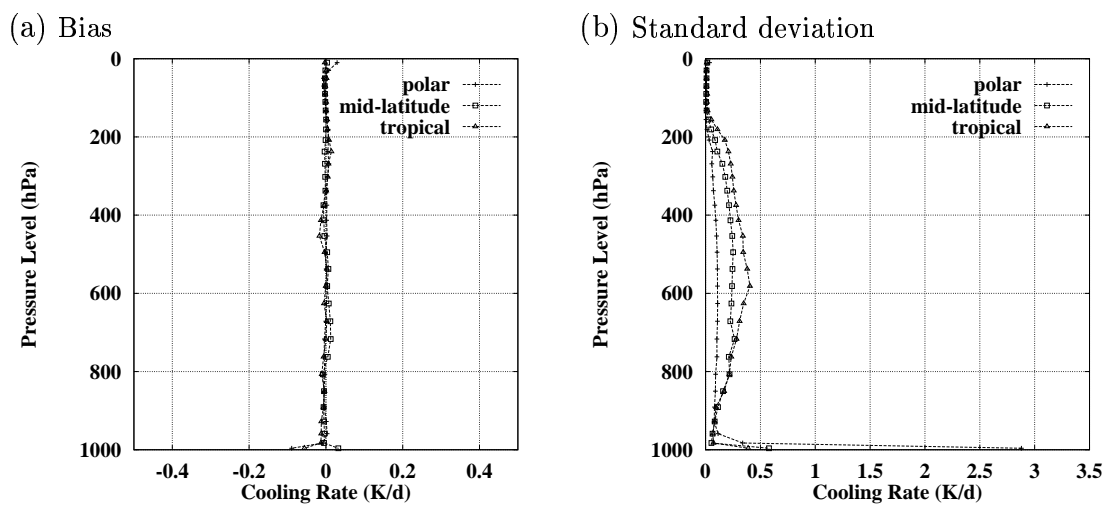
Figure 4: Mean (a) and standard deviation (b) of the comparisons between tangent linear and non-linear clear sky cooling rates, in $K.d^{-1}$. The tangent linear approach uses a single mean Jacobian. The perturbations are taken from the difference between the ECMWF 6- and 12-hour forecasts for 1 July 1998 at 00 UTC. Results are shown in three latitude classes. On (b), the standard deviation of the error in the polar class reaches 3 $K.d^{-1}$ at the surface, whereas they are below 0.6 $K.d^{-1}$ in the other latitudes.
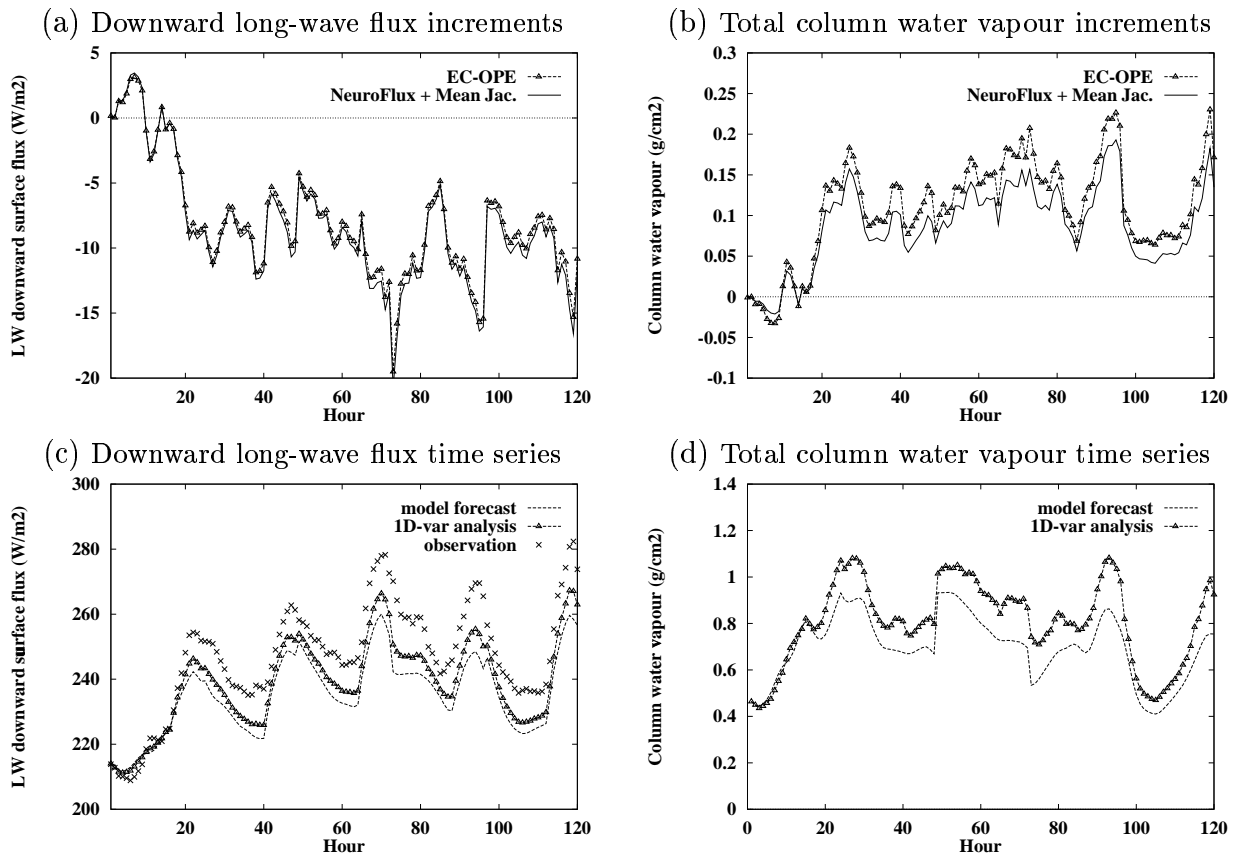
Figure 5: (a) shows the difference between the downward long-wave flux from a 1D-Var analysis using either EC-OPE or the single mean Jacobian approach, and the flux measured at ARM-SGP site by a pyrgeometer. The corresponding time series of total column water vapour increments are shown in (b). Flux and total column water vapour values are presented for EC-OPE on (c) and (d) respectively. In the single mean Jacobian approach, NeuroFlux is used to update the trajectory. The gradient computations are performed with a single mean Jacobian matrix.
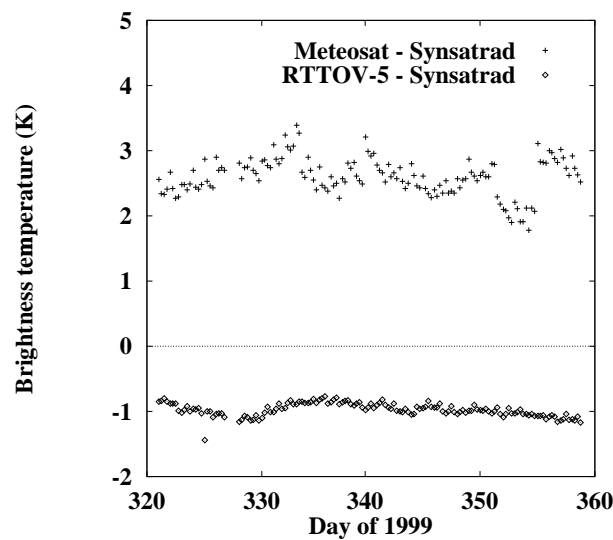
Figure 6: Comparison between the ECMWF 6-hour forecast and the Meteosat-WV observation from 16 November 1999 to 25 December 1999. The 6-hour forecast is converted into Meteosat-WV radiance with either RTTOV or Synsatrad. The upper curve shows the difference between the computation using Synsatrad and the observation. The lower curve shows the difference between the computation using RTTOV and that using Synsatrad.

(a)

(b)
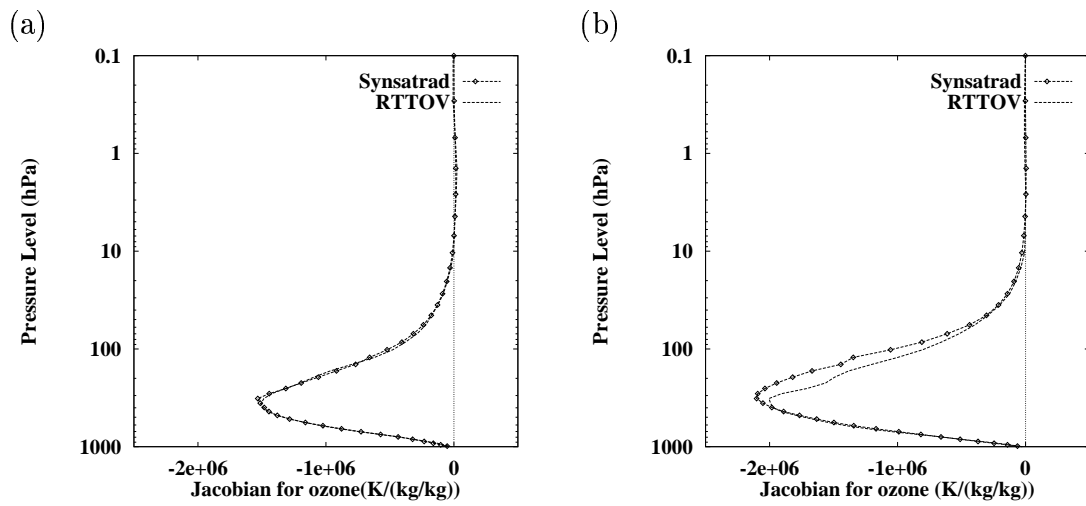
Figure 7: **HIRS-09**. Mean Jacobian for ozone from Synsatrad and RTTOV for the high and mid latitudes (a) and for tropical latitudes (b) at the first iteration of 1D-Var.
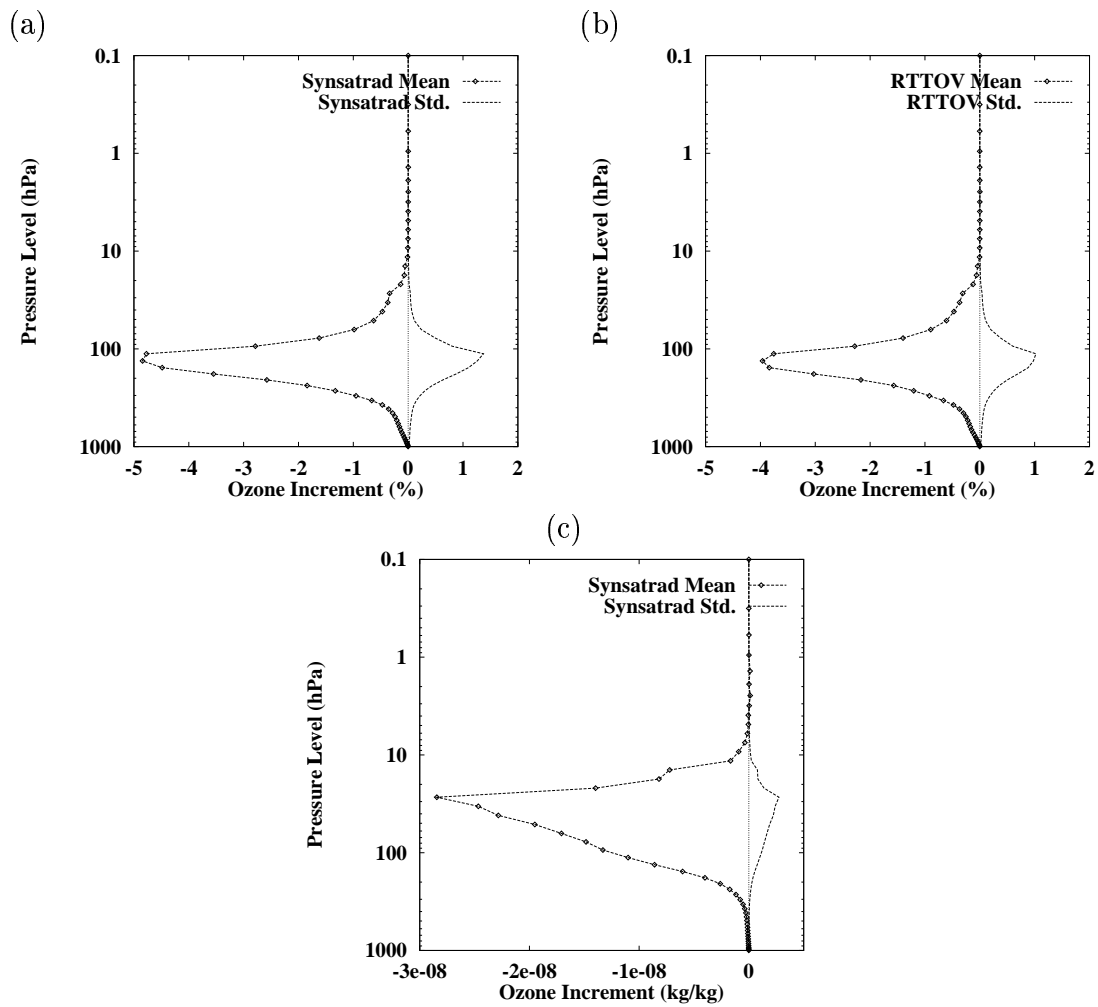
Figure 8: **HIRS-09, tropical latitudes.** Statistics of ozone increments, in %, of Synsatrad (a) and RTTOV (b). The statistics expressed in terms of specific ozone values, in $kg.kg^{-1}$, are shown in (c) for Synsatrad.
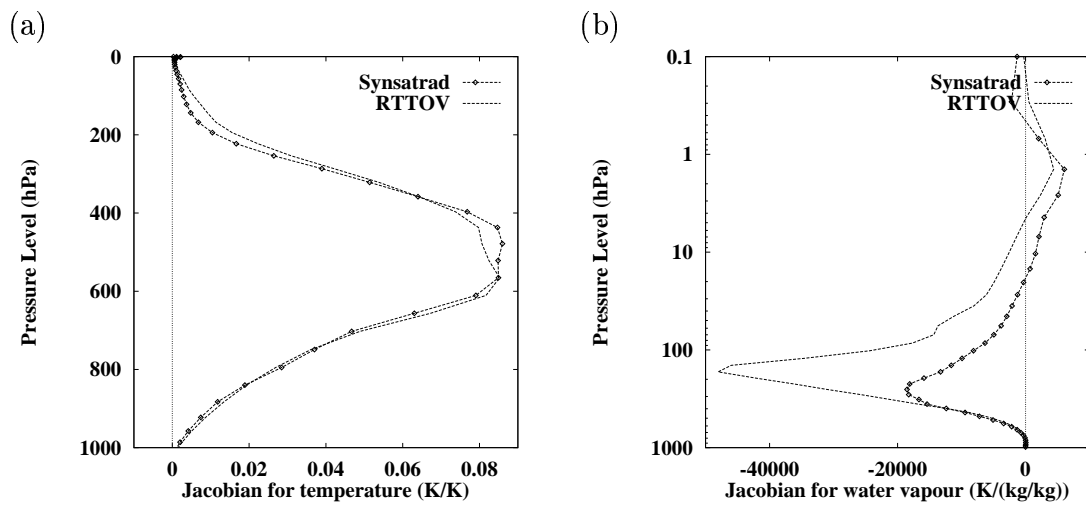
(a)

(b)
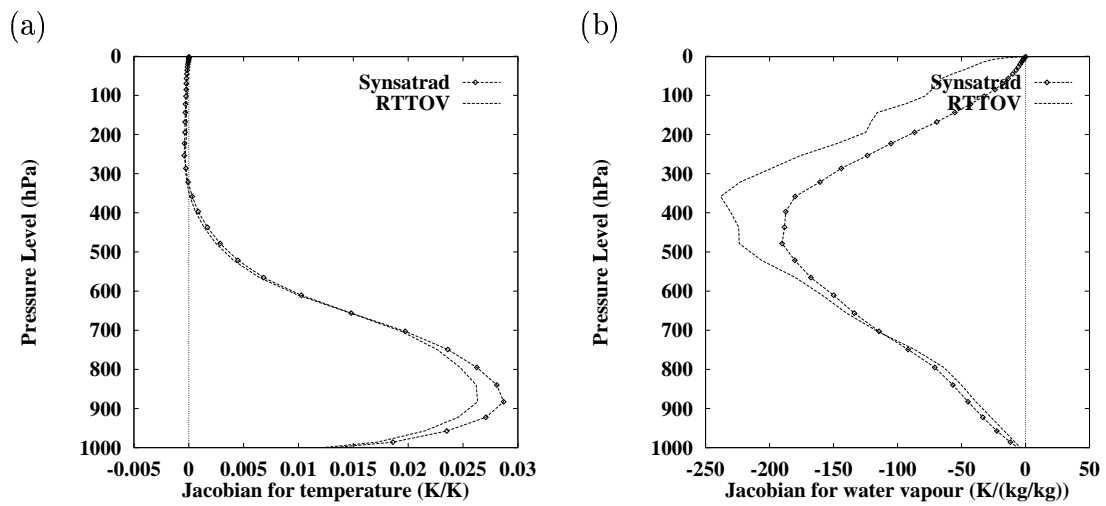
Figure 9: **HIRS-10, high and mid-latitudes**. Mean Jacobians for temperature and water vapour from Synsatrad and RTTOV at the first iteration of 1D-Var.
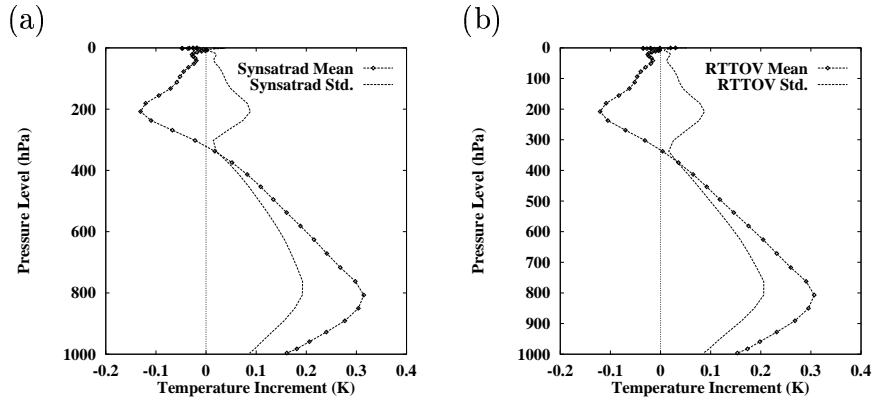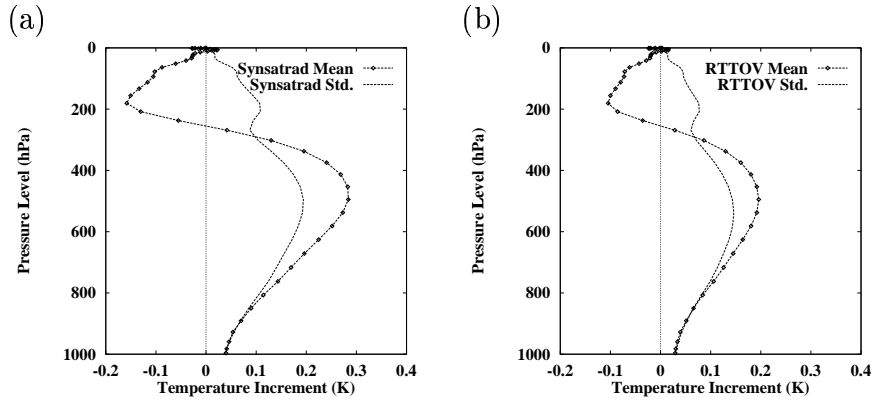
Figure 10: **HIRS-10, high and mid-latitudes**. Statistics of the temperature increments from Synsatrad (a) and RTTOV (b).
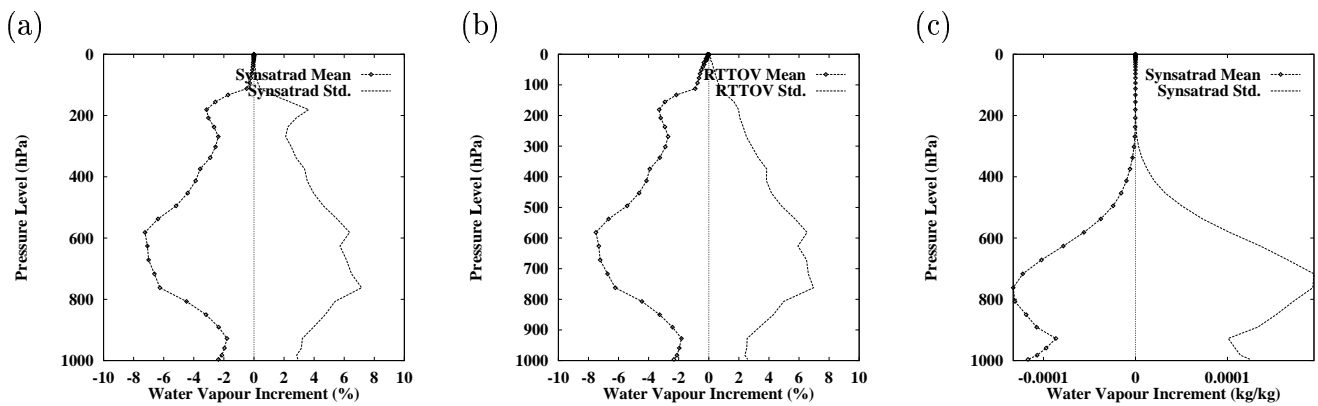
Figure 11: **HIRS-10, high and mid-latitudes**. Statistics of the water vapour increments from Synsatrad (a) and RTTOV-5 (b), in terms of relative change of specific humidity. The statistics in terms of specific humidity are shown in (c) for Synsatrad.

Figure 12: **HIRS-12, high and mid-latitudes**. Mean Jacobians for temperature and water vapour from Synsatrad and RTTOV at the first iteration of 1D-Var.

(a)

(b)

Figure 13: **HIRS-12, high and mid-latitudes**. Statistics of the temperature increments from Synsatrad (a) and RTTOV (b).
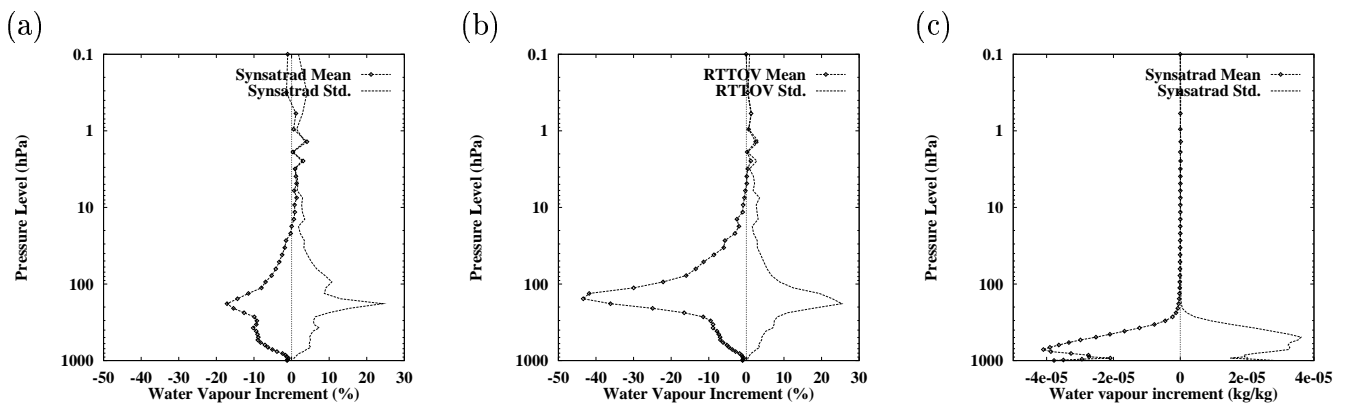
(a)

(b)

(c)

Figure 14: **HIRS-12, high and mid-latitudes**. Statistics of the water vapour increments from Synsatrad (a) and RTTOV-5 (b), in terms of relative change of specific humidity. The statistics in terms of specific humidity are shown in (c) for Synsatrad.
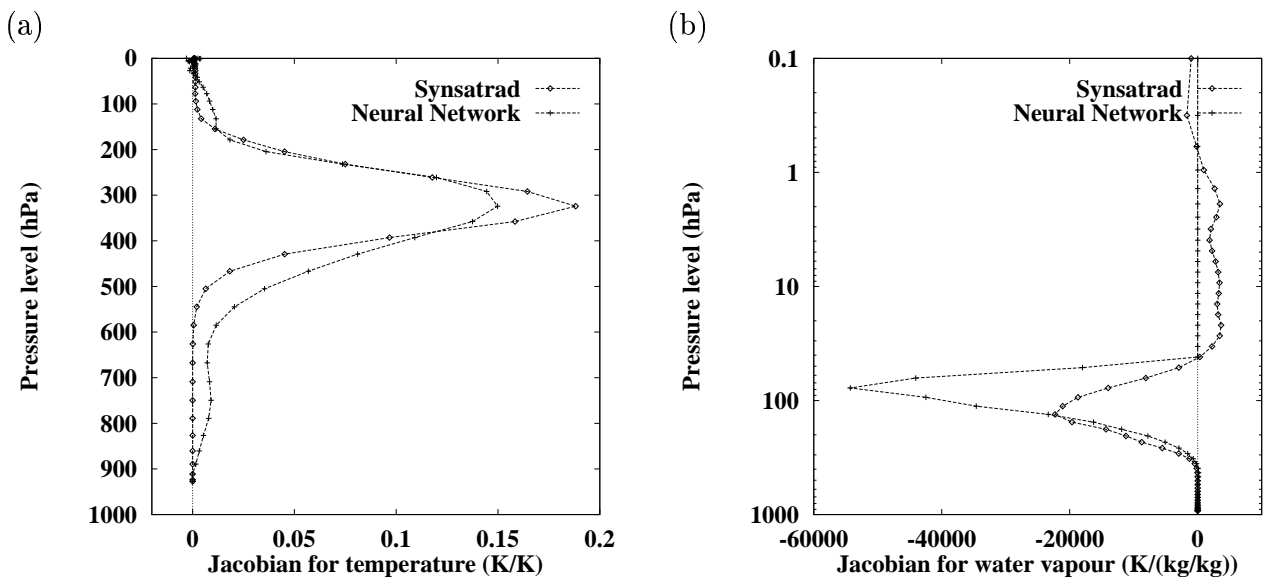
(a)

(b)

Figure 15: **Meteosat-WV**. Illustration of the tests performed to simulate Synsatrad with a formal neural network. Comparison of Synsatrad Jacobians with those of a neural network trained with Synsatrad for a case at latitude 25°N. In order to avoid the scaling problem mentioned in section 4.2, the Jacobian for water vapour is set to zero above 40 hPa. Also the regularisation technique of Aires *et al.* (1999) is used, which allows for smooth Jacobians. The corresponding error in brightness temperature is 0.3 K.